Electronic Supplementary Information

Electrocatalytic H_2 production with a turnover frequency $>10^7$ s^{-1}: The medium provides an increase in rate but not overpotential

Jianbo Hou, Ming Fang, Allan Jay P. Cardenas, Wendy J. Shaw, Monte L. Helm, R. Morris Bullock, John A. S. Roberts* and Molly O'Hagan* [a]

Synthesis of ionic liquids: We synthesized the ionic liquids in a water-free N_2 atmosphere glove box to avoid any hydration during the reaction. High purity dimethylformamide (DMF) and dibutylformamide (DBF) (dry, >99.9%) were filtered through activated alumina prior to use. Sublimation of bis(trifluoromethanesulfonyl)amine ($HNTf_2$, Acros, > 99%) removed impurities from the acid. For a typical synthesis of $[(DMF)H]NTf_2$, we added a small portion of $HNTf_2$ (4.5278 g, 0.0161 mol) to a 20 mL vial containing DMF (1.177 g, 0.0161 mol). A white vapor formed quickly upon adding $HNTf_2$ to DMF due to the vigorous exothermic reaction. A teflon cap sealed the vial until the vapor vanished, followed by adding the next portion of $HNTf_2$. Such steps were repeated several times until the stoichiometry of 1:1 was obtained. The liquid mixture was stirred overnight. Several batches of our synthesized ionic liquids consistently yielded the same color and purity with the expected cation/anion stoichiometry (1:1, error bar < 2%) as confirmed by ^1H, ^{13}C and ^{19}F NMR spectroscopy. NMR diffusometry further confirmed the consistency in transport property (i.e. ion diffusion) among various batches of synthesized protic ionic liquids. The purity of the ionic liquids was also

confirmed by density measurements to confirm the absence of substantial amounts of water in the freshly prepared ionic liquids. Additionally, cyclic voltammetry was used confirm that the ionic liquids were electrochemically silent. The $[(DMF)H]NTf_2$ was a pale yellow color as reported previously. However, the $[(DMF)H]NTf_2$ prepared in this work remained a colorless liquid at room temperature, which crystalizes when in contact with small particles, such as ferrocene, and returns to a liquid phase upon adding water or heating above 70 °C.

Determination of the pK_a of $(DBF)H^+$: The pK_a of $(DBF)H^+$ in acetonitrile was determined using NMR spectroscopy. 0.20 mL of CD_3CN solution of $[(DBF)H]NTf_2$ (50 mM, 10.0 μmol) was added to 0.20 mL of CD_3CN solution of DMF (50 mM, 10.0 μmol) giving a final concentration of 25.0 mM for both the acid and the base. The solution was let to stand for 20 minutes to reach equilibrium. The same procedure was repeated with different initial mole ratios of $(DBF)H^+$ and DMF to determine the equilibrium constant (K_{eq} = [DBF][$(DMF)H^+$]/[$(DBF)H^+$][DMF]) of 0.90 ± 0.01 at 298K. The pK_a of $(DMF)H^+$ in acetonitrile (6.1)[1] was used to calculate the pK_a of $(DBF)H^+$ of 6.1 ± 0.2.

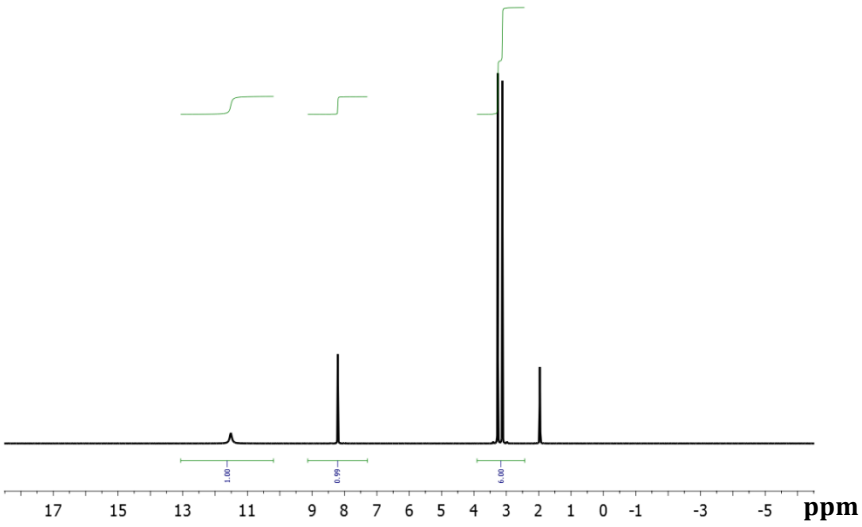

Figure S1: ^{1}H NMR spectrum of $[(DMF)H]NTf_2$ in CD_3CN.

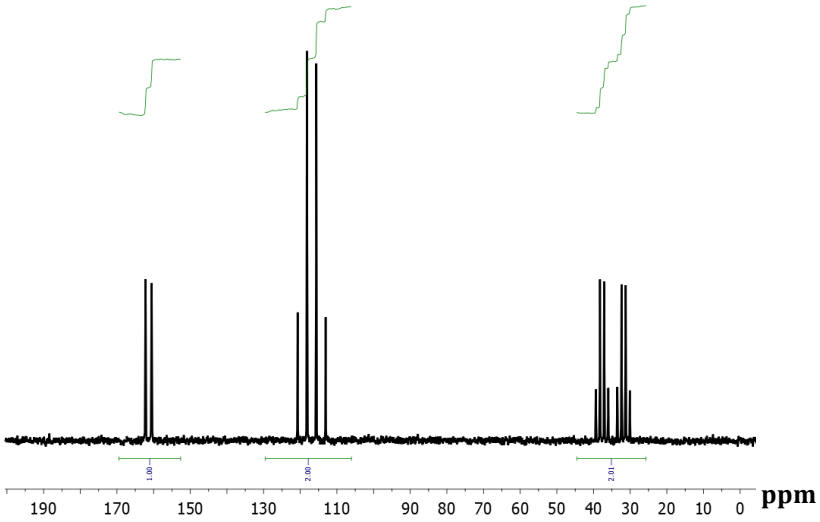

Figure S2: ^{13}C NMR spectrum of neat ionic liquid $[(DMF)H]NTf_2$.

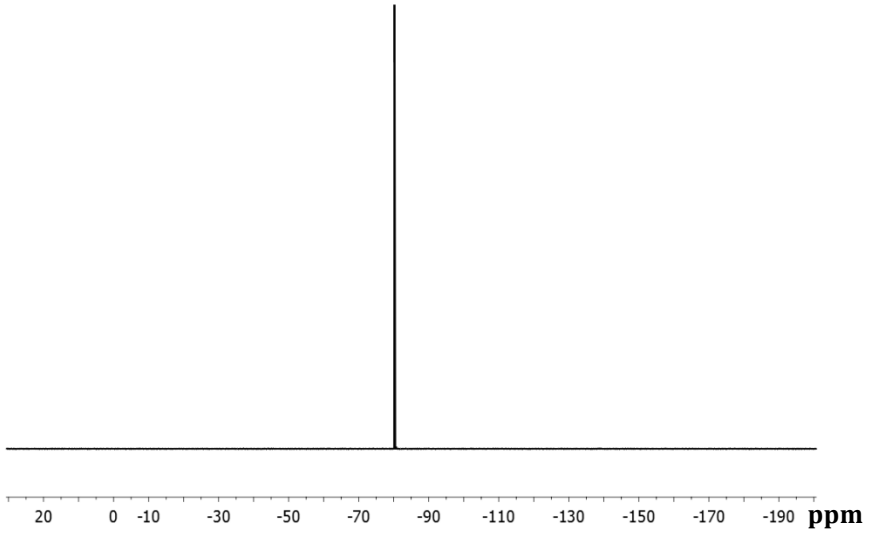

Figure S3: ^{19}F NMR spectrum of neat ionic liquid [(DMF)H]NTf_2.

Cyclic Voltammetry: We conducted cyclic voltammetry experiments on CH instruments 660C potentiostats using a standard three-electrode method. The working electrode was a 1mm glassy carbon disk (Cypress Systems) that was polished for 2 minutes between each scan using Buehler MetaDi® II 0.25 μm diamond paste lubricated with ethylene glycol, followed by rinsing the electrode surface 3 times with MeCN inside the glove box. We then gently wiped out the residual liquid on the electrode surface. A 3mm glassy carbon rod (Alfa Aesar) and a bare platinum wire served as the auxiliary and reference electrodes, respectively. Water was dispensed from a Millipore MilliQ purifier and sparged with nitrogen. A 10 mL syringe allowed adding specific amounts of water into ionic liquids accurately, which was further quantified by ^1H NMR with good consistency. We sealed the electrochemical cell while polishing the electrode to minimize water evaporation for reliable measurements. The uncertainty in the water content is <3% based on ^1H NMR measurements. For each catalyst, the catalytic current i_{cat} plateaued to the steady state

value as the scan rate increased under various catalyst concentrations and water contents. The steady state i_{cat} allowed determination of TOF for each catalyst.

Bulk Electrolysis: Electrocatalytic H_2 production was confirmed by bulk electrolysis of a [(DMF)H]NTf_2 (χ_{H2O} = 0.71) solution containing $[Ni(P^{Ph}{}_2N^{C6H4X}{}_2)_2](BF_4)_2$ (15 μM), X= hexyl, at −1.1 V vs $Fc^{+/0}$, in a bulk electrolysis cell (total volume = 7 mL) charged with 2.1 mL analyte solution. The working electrode was a cylinder of reticulated vitreous carbon. The reference electrode was a glass tube terminating in a Vycor fritted disk and filled with acetonitrile solution of 0.2 M $[Bu_4N]PF_6$ and a silver wire as a reference electrode. The counter electrode is a glass tube terminating in an ultrafine glass filter disk and filled with an acetonitrile solution of 0.2 M $[Bu_4N]PF_6$ (0.2 M) and a Nichrome wire as the counter electrode. Samples of the headspace gas were removed via a gastight syringe during the experiment, and were analyzed by gas chromatography using the detector response calibration to quantify H_2. Gas analysis for H_2 was performed using an Agilent 6850 gas chromatograph equipped with a thermal conductivity detector and fitted with a 10 ft long Supelco 1/8" Carbosieve 100/120 column, calibrated with two H_2/N_2 gas mixtures of known composition. 0.80 C of charge was passed over 2 min, generating 4.0 μmol H_2, corresponding to 96% Faradaic efficiency.

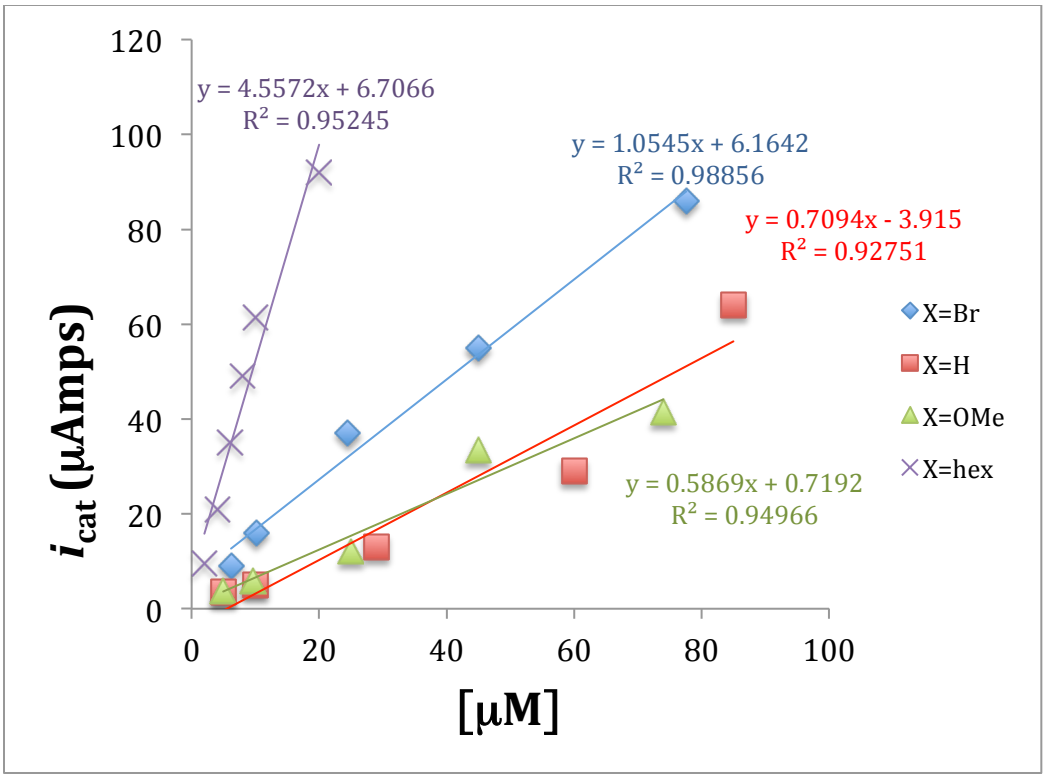

Figure S4. Plot of catalytic current i_{cat} vs. catalyst concentration in [(DMF)H]NTf_2 –H_2O with the water content χ = 0.71 for the $\mathbf{1}^{X}$ family of catalysts. The plot yields linear regression for all the catalysts. The slope of each curve allows the determination of the turnover frequency (TOF) using equation 1.

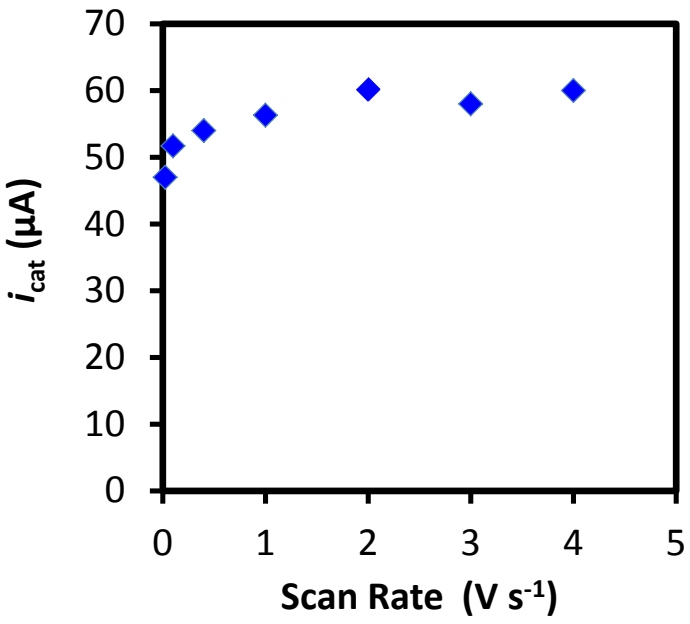

Figure S5: Plot of catalytic current, $i_{cat,}$ vs. scan rate for complex $\mathbf{1}^{\mathbf{hex}}$ in [(DMF)H]NTf_2 –H_2O with the water content $\chi = 0.71$.

NMR spectroscopy: NMR data were recorded on a 500 MHz ^{1}H frequency Agilent VNMRS equipped with a direct detect dual band probe (Agilent OneNMR probe) and a Performa IV gradient amplifier with maximum gradient output of 80 G/cm or a 300 MHz ^{1}H frequency Agilent VNMRS equipped with a direct detect dual band probe and a Performa II gradient amplifier with maximum gradient output of 20 G/cm. The VNMRJ standard DOSY pulse sequence was used for all diffusion measurements. The NMR signal attenuates as described by the Stejskal-Tanner equation[2]:

$$I = I_0 e^{-D\gamma^2 g^2 \delta^2 (\Delta - \frac{\delta}{3})} \quad (1)$$

Where I_0 denotes the signal intensity in the absence of gradient, γ is the gyromagnetic ratio of the studied nuclei, g is the gradient strength, δ is the gradient pulse duration and

Δ is the time interval between two gradient pairs. The pulse sequence used a π/2 pulse of 8.8 μs and π pulse of 17.6 μs, δ = 2-4 ms and Δ = 200 – 800 ms, depending on sample concentrations and water contents. In our measurements, we varied gradient strength from 0 to 80 G/cm or 0 to 20 G/cm in 10 steps with 16 or 32 scans at each step. Normal signal attenuation (> 80% signal decay) yielded single diffusion coefficient fits for all our measurements, with an experimental error < 5%.

^{1}H DOSY experiments were used to determine D_{cat}; however, low catalyst solubility in [(DMF)H]NTf_2–H_2O limited direct measurement of D_{cat}. To determine D_{cat} in this medium, we accurately measured D_{cat} for each catalyst in [(DBF)H]NTf_2–H_2O and scaled D_{cat} to its corresponding value in [(DMF)H]NTf_2–H_2O, assuming the D_{cat} behavior in the two ionic liquids follows the same trend as D_{H+} and D_{NTf2}, which vary identically over the range of water concentrations by a factor of three between the two ionic liquids (*Figure S6 and S7*). The acidic proton is located on the dialkylformamide in the dry ionic liquids but exchanges with added H_2O, causing peak averaging in the ^{1}H NMR spectrum. The measured D_{H+} values then average over all ^{1}H environments sampled on the measurement timescale (~10^2 ms) and are thus lower bounds on the actual transport coefficients for the proton which may be further accelerated by the Grotthuss mechanism (structural diffusion).[3-5]

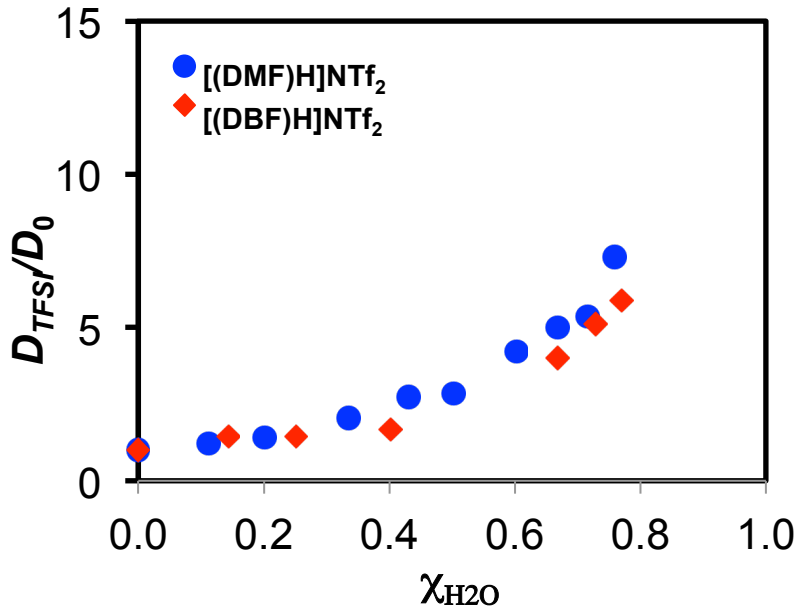

Figure S6. Plot of the normalized diffusion coefficient for the NTf_2 anion, D_{NTf2}/ D_0 where $D_0 = D_{NTf2}$ with no added water, vs. mole faction of water for the [(DMF)H]NTf_2–H_2O in blue and the [(DBF)H]NTf_2–H_2O in red. The plot shows the uniform increase in diffusion as the water content is increased.

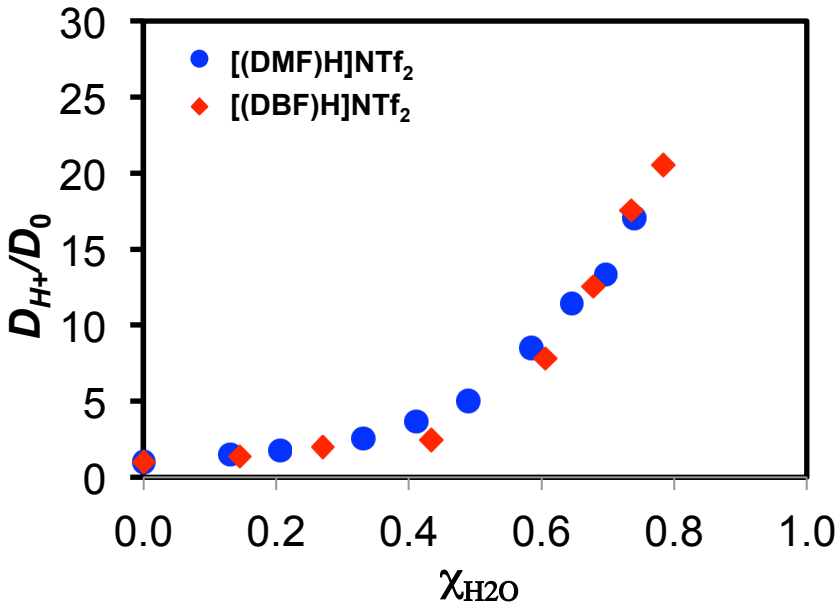

Figure S7. Plot of the normalized diffusion coefficient for the H^+/H_2O, D_{H+}/ D_0 where $D_0 = D_{H+}$ with no added water, vs. mole faction of water for the [(DMF)H]NTf_2–H_2O in blue and the [(DBF)H]NTf_2–H_2O in red. The plot shows the uniform increase in diffusion as the water content is increased.

Table S1: Diffusion coefficients in [(DMF)H]NTf_2-H_2O and [(DBF)H]NTf_2-H_2O, χ = 0.71.

	[(DMF)H]NTf_2-H_2O χ_{H2O} **= 0.71** ***D*** **(10^{-11} m^2/s)**	**[(DBF)H]NTf_2-H_2O** χ_{H2O} **= 0.71** ***D*** **(10^{-11} m^2/s)**
H^+/H_2O	36	17
$DMFH^+$ or $DBFH^+$	14	3.9
NTf_2^-	10	3.9
$\mathbf{1}^{hex}$	3.0*	1.0
$\mathbf{1}^{Br}$	3.9*	1.3
$\mathbf{1}^{OMe}$	3.9*	1.3
$\mathbf{1}^{H}$	4.8*	1.6

*Calculated from [(DBF)H]NTf_2-H_2O values.

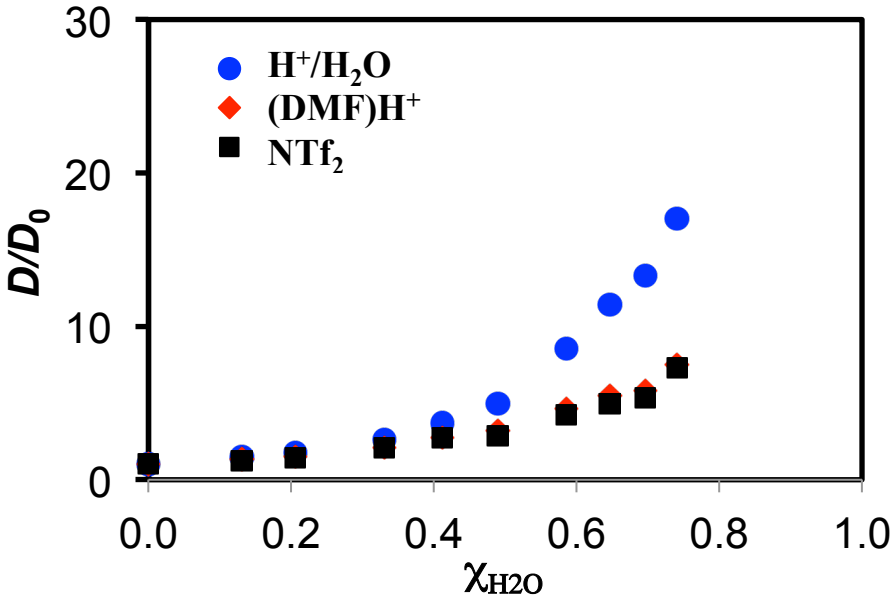

Figure S8: Normalized ratio of diffusion coefficients for all species in [(DMF)H]NTf_2–H_2O vs. mole faction of water.

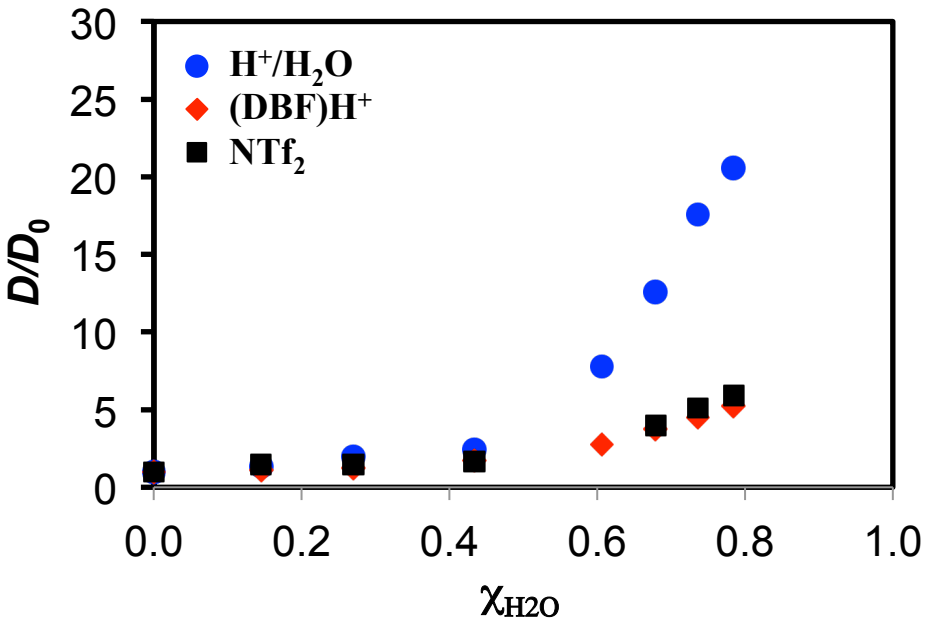

Figure S9: Normalized ratio of diffusion coefficients for all species in [(DBF)H]NTf_2–H_2O vs. mole faction of water.

Determination of Open Circuit Potential in protic ionic liquids: The measurement of open circuit potential (OCP) in the protic ionic liquids employed the same experimental protocol as reported previously.[6, 7] We immersed a platinum wire in aqua regia for 30 min, rinsed it with 18 MΩ H_2O and heated it to orange glow using H_2/air flame prior to transferring it to the glovebox under an N_2 atmosphere. The analyte solution containing [(DMF)H]NTf_2–H_2O mixture and ferrocenium tetrafluoroborate (< 1 mg) was sparged with high purity H_2 for 20 min before any measurement. We then measured the OCP between the platinum wire and a AgCl/Ag pseudoreference electrode containing MeCN (0.2 M NBu_4PF_6) separated from the analyte solution by a Vycor frit. The analyte solution remained stirring for 40 s during the OCP measurement. Then the stirring was shut off to measure the potential of the AgCl/Ag electrode vs. the $Cp_2Fe^{+/0}$ couple voltammetrically using glassy carbon working and counter electrodes in a three-electrode

configuration. The measured OCP remained stable with a variation < 0.2 mV. Water evaporation over the measurement was negligible as confirmed by ^{1}H NMR, with an error bar < 1%.

Table S2: Values for the equilibrium potentials for the interconversion of protons and electrons with H_2 (E_{H+}) as determined by open circuit potential measurements, and catalytic potentials ($E_{cat/2}$) and calculated overpotentials (η) for complex $\mathbf{1}^{\mathbf{hex}}$ as the mole faction of water is increase in the [(DMF)H]NTf_2–H_2O ionic liquid.

χ_{H2O}	E_{H+} (V)	$E_{cat/2}$ (V)	η (V)
0.46	-0.0403	-0.493	0.45
0.58	-0.100	-0.540	0.44
0.62	-0.1278	-0.600	0.47
0.71	-0.180	-0.590	0.41

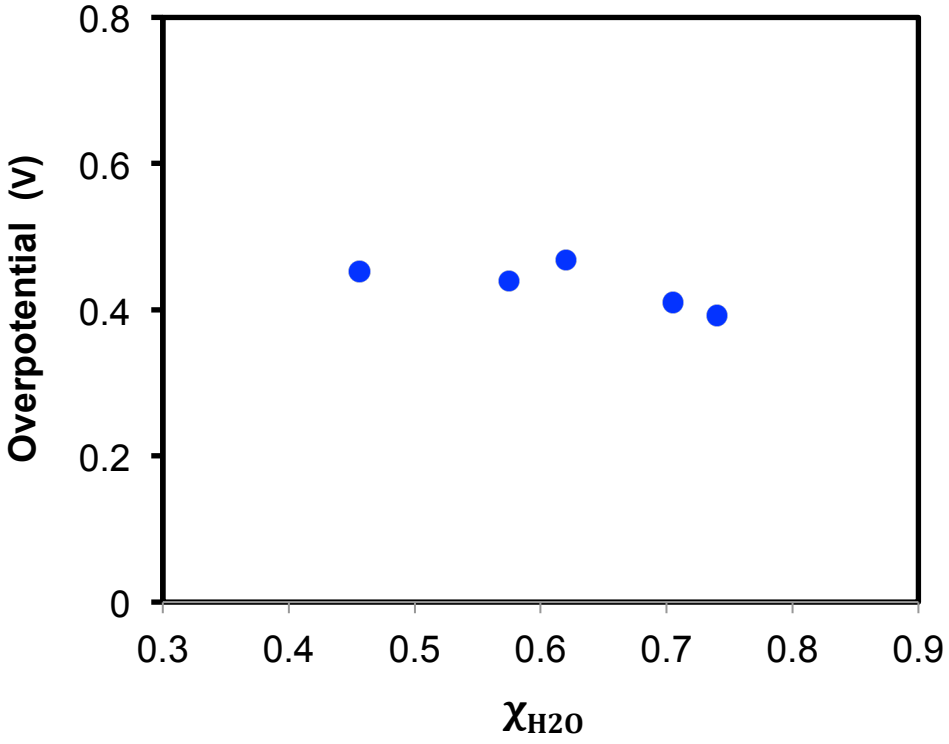

Figure S10: Plot of the change in overpotential vs. mole faction of water for complex $\mathbf{1}^{hex}$ in the [(DMF)H]NTf_2–H_2O ionic liquid. Minimal net change in overpotential is observed with added water because the equilibrium and the catalytic potentials both shift more negative. The negative shift in E_{H+} is expected since water is acting as a base in these systems. The shift in the catalytic potential is attributed to the coupling of the proton and electron transfer reactions, which is dependent on pH. This behavior is consistent with other systems reported in the literature.[8,9]

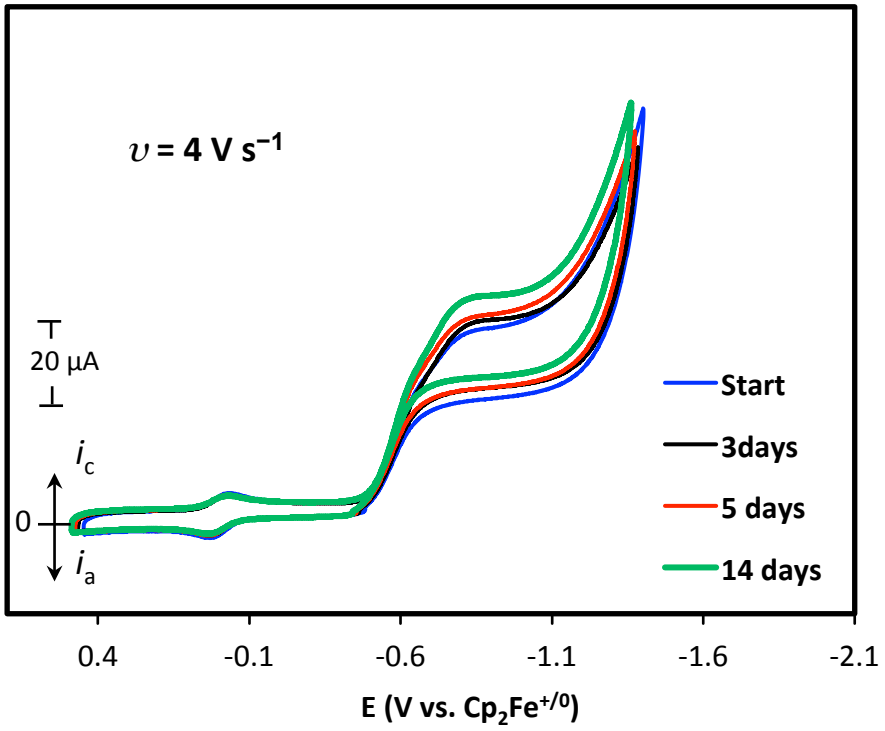

Figure S11: Overlay of cyclic voltamagrams of complex $\mathbf{1}^{\mathbf{hex}}$ taken from 0-14 days, showing no loss in catalytic current over time in [(DMF)H]NTf_2–H_2O.

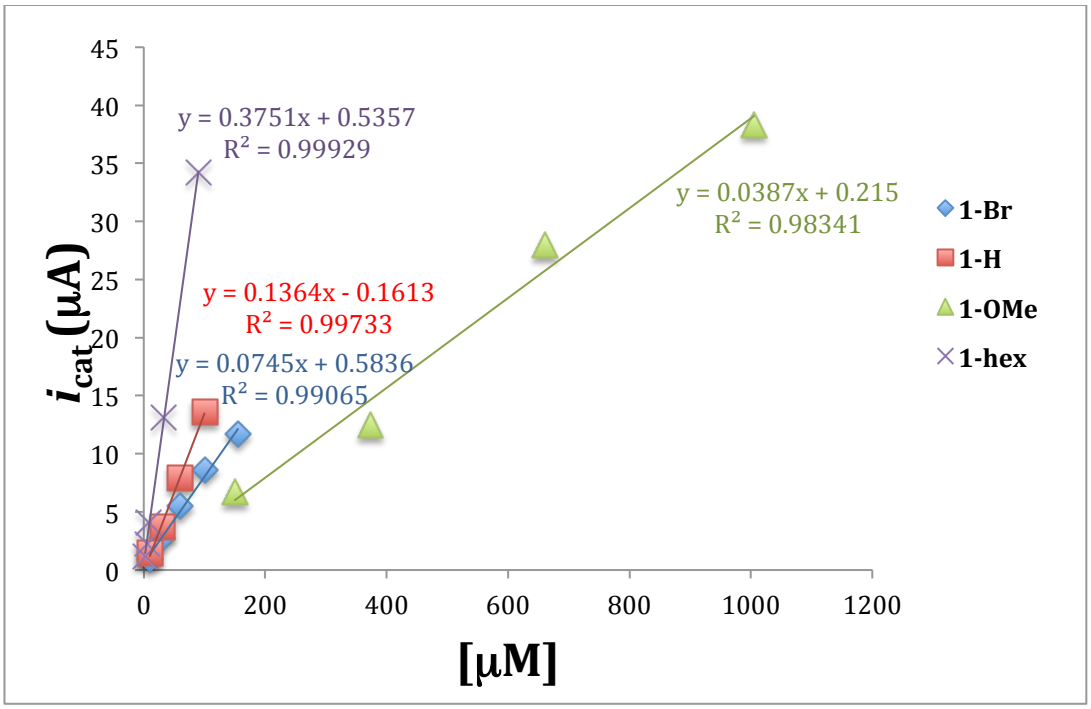

Figure S12. Plot of catalytic current i_{cat} vs. $\mathbf{1}^{X}$ catalyst concentration in [(DBF)H]NTf_2–H_2O with the water content χ = 0.71. The plot yields a linear regression for all the catalysts. The slope of each curve allows the determination of the turnover frequency (TOF) using equation 1. TOF values are adjusted from those reported in reference 14 resulting from the determination of more accurate D_{cat} values, among other factors.

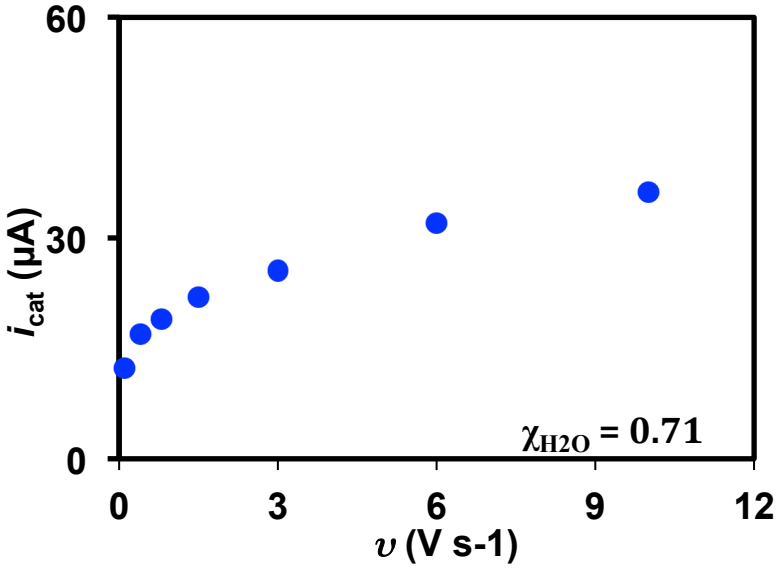

Figure S13: Plot of catalytic current, $i_{cat,}$ vs. scan rate for complex $\mathbf{1}^{hex}$ in [(DBF)H]NTf_2–H_2O with water content χ = 0.71.

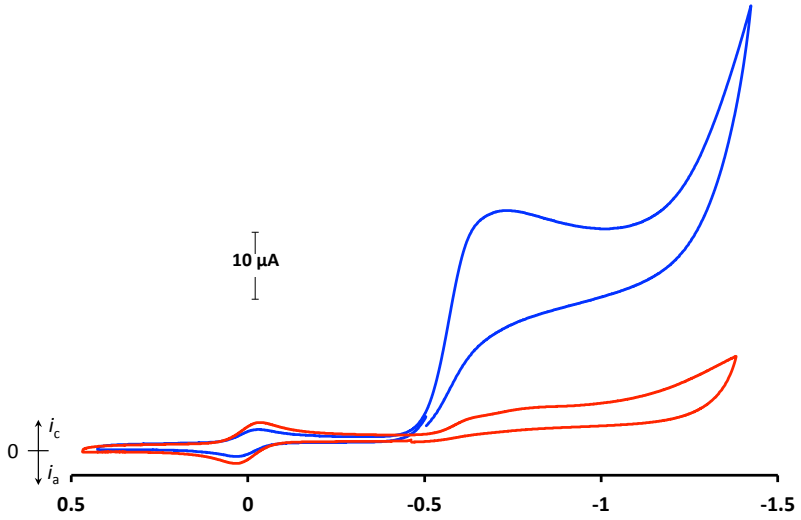

Figure S14: Cyclic voltammograms of 8 µM 1^{hex} comparing the catalytic current observed in [(DMF)H]NTf_2-H_2O (χ_{H2O} = 0.71), blue, and [(DBF)H]NTf_2-H_2O (χ_{H2O} = 0.71), red, with a scan rate of 0.4 V s^{-1}.

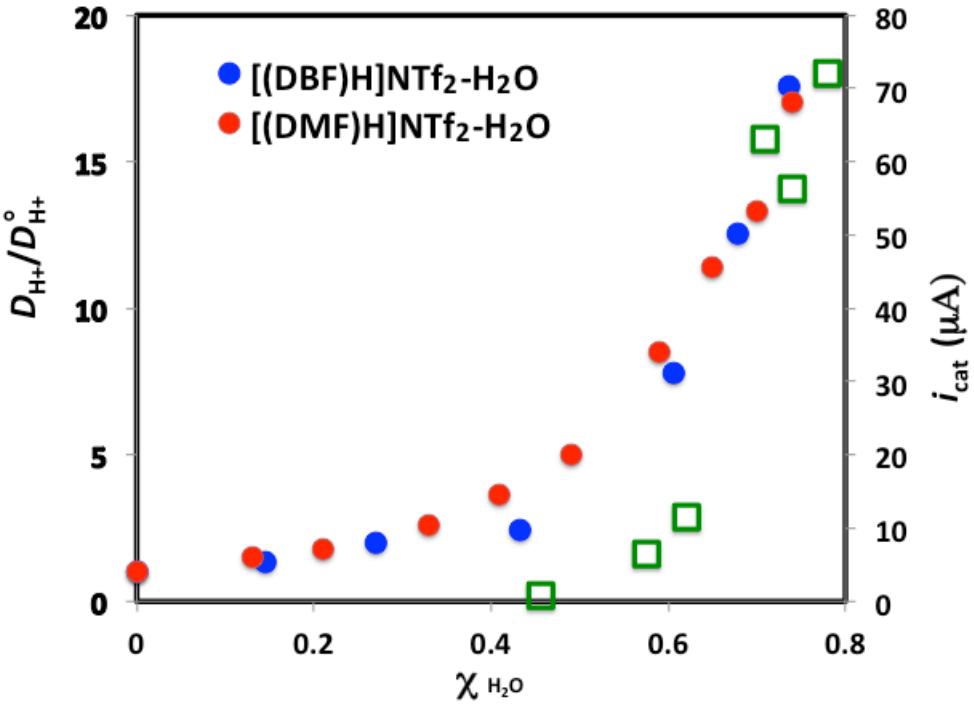

Figure S15: Proton diffusion coefficients vs. χ_{H2O} (left ordinate; normalized by dividing D_{H+} by D^0_{H+}, the value with no added water) for [(DMF)H]NTf_2-H_2O (red circles) and [(DBF)H]NTf_2-H_2O (blue circles); i_{cat} measured with $\mathbf{1}^{hex}$ in [(DMF)H]NTf_2-H_2O vs χ_{H2O} (green squares, right ordinate).

References

1. I. M. Kolthoff, M. K. Chantooni, Jr. and S. Bhowmik, *Anal. Chem.*, 1967, **39**, 1627-1633.
2. E. O. Stejskal and J. E. Tanner, *J. Chem. Phys.*, 1965, **42**, 288-292.
3. D. Marx, M. E. Tuckerman, J. Hutter and M. Parrinello, *Nature*, 1999, **397**, 601-604.
4. S. N. Suarez, J. R. P. Jayakody, S. G. Greenbaum, T. Zawodzinski and J. J. Fontanella, *J. Phys. Chem. B*, 2010, **114**, 8941-8947.
5. S. Cukierman, *Biochim. Biophys. Acta, Bioenerg.*, 2006, **1757**, 876-885.
6. D. H. Pool, M. P. Stewart, M. O'Hagan, W. J. Shaw, J. A. S. Roberts, R. M. Bullock and D. L. DuBois, *Proc. Natl. Acad. Sci. U.S.A.*, 2012, **109**, 15634-15639.
7. J. A. S. Roberts and R. M. Bullock, *Inorg. Chem.*, 2013, **52**, 3823-3835.
8. A. M. Appel, D. H. Pool, M. O'Hagan, W. J. Shaw, J. Y. Yang, M. Rakowski DuBois, D. L. DuBois and R. M. Bullock, *ACS Catal.*, 2011, **1**, 777-785.
9. P.A. Jacques, V. Artero, J. Pecaut, M. Fontecave. *Proc. Natl. Acad. Sci*. **2009**, *106*, 20627–20632.